energies

Article

Extended Permanent Magnet Synchronous Motors Speed Range Based on the Active and Reactive Power Control of Inverters

Pham Quoc Khanh [1,*], Viet-Anh Truong [2] and Ho Pham Huy Anh [3]

[1] Faculty of Electrical Engineering Technology, Industrial University of Ho Chi Minh City (IUH), Ho Chi Minh City 70000, Vietnam
[2] Faculty of Electrical and Electronics Engineering, University of Technology and Education, Ho Chi Minh City 70000, Vietnam; anhtv@hcmute.edu.vn
[3] Ho Chi Minh City University of Technology (HCMUT), 268 Ly Thuong Kiet Street, District 10, Ho Chi Minh City 70000, Vietnam; hphanh@hcmut.edu.vn
* Correspondence: phamquockhanh@iuh.edu.vn; Tel.: +84-934-093-716

Abstract: The paper proposes a new speed control method to improve control quality and expand the Permanent Magnet Synchronous Motors speed range. The Permanent Magnet Synchronous Motors (PMSM) speed range enlarging is based on the newly proposed power control principle between two voltage sources instead of winding current control as the conventional Field Oriented Control method. The power management between the inverter and PMSM motor allows the Flux-Weakening obstacle to be overcome entirely, leading to a significant extension of the motor speed to a constant power range. Based on motor power control, a new control method is proposed and allows for efficiently reducing current and torque ripple caused by the imbalance between the power supply of the inverter and the power required through the desired stator current. The proposed method permits for not only an enhanced PMSM speed range, but also a robust stability in PMSM speed control. The simulation results have demonstrated the efficiency and stability of the proposed control method.

Keywords: permanent magnet synchronous motors (PMSM); active power control; reactive power control; extended speed range; ripple torque reduction; flux-weakening (FW)

check for updates

Citation: Khanh, P.Q.; Truong, V.-A.; Anh, H.P.H. Extended Permanent Magnet Synchronous Motors Speed Range Based on the Active and Reactive Power Control of Inverters. *Energies* **2021**, *14*, 3549. https://doi.org/10.3390/en14123549

Academic Editor: Nicu Bizon

Received: 10 May 2021
Accepted: 9 June 2021
Published: 15 June 2021

Publisher's Note: MDPI stays neutral with regard to jurisdictional claims in published maps and institutional affiliations.

Copyright: © 2021 by the authors. Licensee MDPI, Basel, Switzerland. This article is an open access article distributed under the terms and conditions of the Creative Commons Attribution (CC BY) license (https://creativecommons.org/licenses/by/4.0/).

1. Introduction

Permanent Magnet Synchronous Motors (PMSM) are increasingly widely used in civil and industrial applications because of their high efficiency, high power density, low maintenance cost, and lower permanent magnet price. The vector control method's popularity, including Field Oriented Control (FOC) [1–6] and Direct Torque Control (DTC) [7–10], stems from its advantages of simplicity in the control structure, ease of operation, reliability, and high efficiency [11,12].

There are two main parts of the operating speed range of PMSM operation, including constant torque range and constant power range, as mentioned in Figure 1. The speed control principle in the constant torque region (in which the PMSM rotor speed is below the rated speed) is suitable for the vector control method when the operating voltage is lower than the inverter output voltage limit. When the PMSM speed exceeds the rated speed, the Back Electromotive Force (B-EMF) generated in the winding, caused by a permanent magnet flux on the rotating rotor in the lumen of the stator windings, can increase beyond the limit of the voltage of the inverters. For motors that do not use permanent magnets, such as induction motors, reducing the current rotor windings can reduce the BEMF voltage [13–15]. Unfortunately, this way is not possible with rotor motors that use permanent magnets. Due to the limit of output voltage, the inverter cannot increase the voltage to stabilize the stator current control.

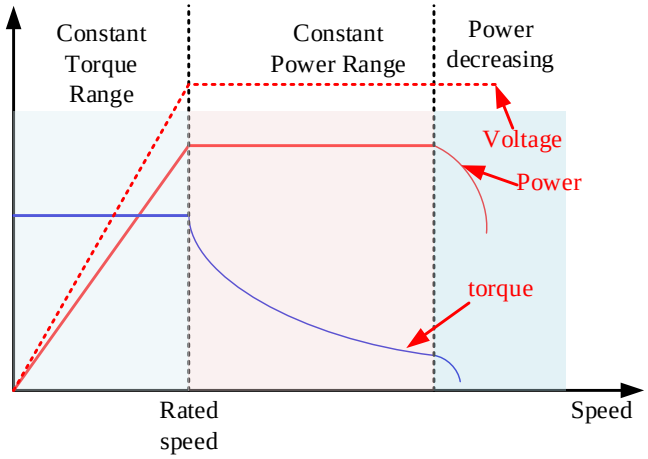

Figure 1. The operating speed range of PMSM.

The input DC voltage is proportional to the maximum amplitude of the output voltage of the inverter. Therefore, in some studies, the expansion of the motor operating speed is achieved by increasing the inverter input voltage [16,17]. However, the step-up voltage method encounters the main limitation of expanding the power drive room for DC–DC voltage converter circuits, and only changes in a narrow speed range. In addition, inverters are designed to operate within a specific voltage limit. Increasing DC voltage to increase motor speed increases inverter costs in applications requiring a high-speed operation.

To ensure that the active power is transmitted to the motor, the reactive power is drawn out of the inverter to ensure that a low voltage amplitude source can push power into a higher voltage source. Then, the d-axis current increases the negative amplitude during entering the FW region, which manifests reactive power inflowing from the PMSM to the inverter.

On the other hand, during operation in the FW zone, the inverter voltage cannot exceed the inverter output voltage limit. However, controlling the stator current using current controllers will cause the estimated controller output voltage to exceed a given boundary. This trouble leads to an increased stator current ripple, resulting in increasing electromagnetic torque ripple and reducing the efficiency in reference velocity tracking.

Several improvements have been used in PMSM speed control in FW to improve control efficiency and reduce current ripple during voltage limit violation in the FW zone. These methods include the Auto-tuning method [18–20], Fuzzy Logic Speed Control [21–25], Improved UDE-Based Flux-Weakening Control [26], and Single Current Regulator Control [27–30].

When entering the FW zone, the d-axis current is adjusted to increase negatively based on the PI controller, where input is the deviation between the maximum voltage amplitude supplied by the inverter and the voltage at the current controller output. As the voltage fluctuation is more extensive in the FW region, the d-axis current ripple also increases. The fuzzy logic speed control method reduces the d-axis current ripple desired by replacing a PI controller with a Fuzzy PI controller. The Fuzzy PI current controller's output voltage is less violated than the PI current controller, leading to a reduced ripple of the d-axis current component. However, this violation's nature persists and adversely affects the control quality when the current controller output voltage estimated value still exceeds the limit voltage value of the inverter.

Single Current Regulator Control approach allows elimination of the output voltage violation when the voltage amplitude is kept at the rated value, as shown in [29]. However, the voltage angle change is based on a current error, without considering the inverter power balance and the load power caused by the wave. Results are demonstrated in [29], on the proposed solutions of Single Current Regulator Control method proposed in [27,31].

Research [29] can only minimize power imbalance by limiting voltage angle variation, but does not wholly address the power imbalance's harmful effects.

Another creative direction in minimizing current and torque ripple in the FW region aims to optimize the current controller parameters. The PSO algorithm is used in [32] to find suitable values when working conditions were changed. A Fuzzy-PI controller is used instead of the PI controller in the more refined determination of the d-axis reference current when the motor operates in the FW region. These innovative methods minimize output torque ripple, while reducing the reference current's effect on the control voltage. However, these methods increase the complexity, and require an amount of computation in the speed control process of PMSM.

The novelty and contributions of this paper are tri-fold. Firstly, this paper proposes the new PMSM speed control based on balancing the output inverter energy and the motor's load energy. The proposed approach differs from the known solution because it does not use rated speed to switch from a constant torque region to an FW region. A change in reactive power leads to a change in rotor speed. Second, the energy transformation to the machine is done by sending energy between two voltage sources, the inverter output voltage and the BEMF of the motor. Eventually, a detailed analysis of the power transmission principle between the two voltage sources is discussed in the following section.

Over the entire operating speed range of the PMSM, the increase (or decrease) of the rotor speed is accomplished by increasing (or decreasing) the active power of the inverter, which enables the roaming to operate without the need to switch different control methods between the two operating zones. Power control will minimize current and torque ripple, and the power supplied to the PMSM will also better monitored. This advantage is especially significant in mobile systems with batteries. The new control method allows efficient reduction of the electric current and torque ripples in the motor through direct control of the inverter output voltage.

The remainder of this paper is structured as such: Part 2 presents the PMSM math model and the principle of transferring power from the inverter to the PMSM; Part 3 introduces the principle of controlling a PMSM motor's speed based on the active power control; Part 4 shows the results obtained after the simulation modeling for the proposed algorithm with the Direct Current Calculation and Vector Current Control algorithms used in the comparison; Part 5 includes the conclusion.

2. Speed Control of PMSM Drive Systems

2.1. PMSM Model and Its Limitations

According to [33], Equations (1) and (2) show the relationship between stator voltage, stator current, and rotor speed. The dq coordinate system is performed through the Park transformation, converting from the *abc* three-dimensional space to the dq two-dimensional space with almost constant values.

$$v_d = R_S \times i_d + L_d \times \frac{i_d}{dt} - Pp \times \omega_m \times L_q \times i_q \quad (1)$$

$$v_q = R_S i_q + L_q \frac{i_q}{dt} + Pp.\omega_m.L_d.i_d + Pp.\omega_m.\lambda_{pm} \quad (2)$$

where v_d, v_q, i_d and i_q are the components voltage and current on the dq-axis, respectively. L_d and L_q are the stator coil inductance components in the dq coordinate system, λ_{pm} is the flux linkage of the permanent magnet on the rotor, R_S is the coil resistance, ω is the rotor speed, and Pp is the number of pole pairs.

When analyzing the PMSM in the stationary state, the current variation is zero; the voltage Equations are rewritten in (3) and (4).

$$v_d = R_S \times i_d - Pp \times \omega_m \times L_q \times i_q \quad (3)$$

$$v_q = R_S \times i_q + Pp \times \omega_m \times L_d \times i_d + Pp \times \omega_m \times \lambda_{pm} \quad (4)$$

Electromagnetic torque is determined by (5)

$$T_e = \frac{3}{2} \times Pp\left(\lambda_{pm} \times i_q + \left(L_d - L_q\right) \times i_q \times i_d\right) \quad (5)$$

According to Newton's Second Law for Rotation, the rotational acceleration of the rotor is determined by (6).

$$\frac{d\omega_m}{dt} = \frac{1}{J}(T_e - T_L - F\omega_m) \quad (6)$$

where:

J: The inertia of motor and load combined referred to the motor shaft.
F: The combined viscous friction coefficient of rotor and load.
θ: Rotor angular position.
T_L: Shaft load torque.
θm: Angular velocity of the rotor (mechanical speed)

During operation, the stator voltage and current are limited below their rated values. The voltage limit is determined based on the motor insulation capacity and the maximum voltage amplitude generated by the inverter, determined by the dc bus voltage. Current limits are usually related to the motor heat dissipation, and the manufacturer provides its value. The Equations described the limits of voltage and current are expressed through (7) and (8), respectively:

$$v_d^2 + v_q^2 = v_s^2 \le v_{s,max}^2 \quad (7)$$

$$i_d^2 + i_q^2 = i_s^2 \le i_{s,max}^2 \quad (8)$$

where v_s represents the vector amplitude of the stator voltage, $v_{s,max}$ is the maximum output voltage of the inverter, i_s is the vector amplitude of the stator current, and $i_{s,max}$ denotes the maximum output current of the inverter.

When the PMSM motor speed exceeds the rated speed, it is possible to ignore the voltage drop on the stator coil since they are insignificant in comparison to the back EMF on the stator winding. On the other hand, in the steady-state, the flux linkage is considered constant, resulting in the derivative of the current to zero $(di_d/dt = 0; di_q/dt = 0)$. Therefore, the stator voltage Equations in (1) and (2) are rewritten as follows:

$$v_d = -\omega_e L_q i_q \quad (9)$$

$$v_q = \omega_e L_d i_d + \omega_e \lambda_{pm} \quad (10)$$

Substitute (9) and (10) into (7), the stator voltage limit in the constant power region is described by (11).

$$\left(L_q i_q\right)^2 + \left(L_d i_d + \lambda_{pm}\right)^2 \le \frac{v_{s,max}^2}{\omega_e^2} \quad (11)$$

The voltage and current restriction relationships of the IPMSM in the whole region are shown in Figure 2, which indicates both of the voltage-limiting circle and current-limiting circle.

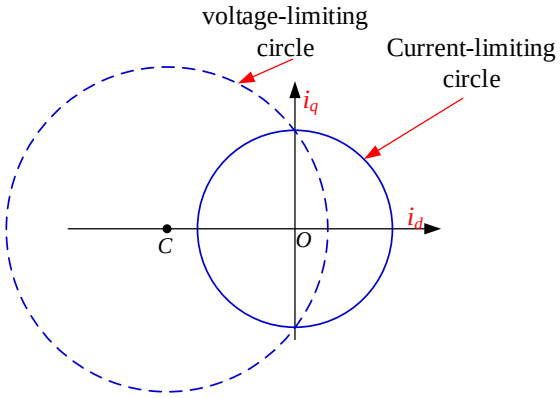

Figure 2. Operating regions of PMSM in dq component current plane.

2.2. Principle of Transferring Power from the Inverter to the Motor

Consider the static state of the PMSM working with speed ω_1 and electromagnetic torque T_{e1}. the electromagnetic torque must balance with the load torque (friction torque included) to keep the speed constant. At this time, the motor provides the power P_1 ($P_1 = \omega_1 \times T_{e1}$). Ignore the energy conversion losses and the stator winding losses, and the PMSM power consumption is equal to the inverter's electrical power.

The inverter needs to provide a power P_2 ($P_2 = \omega_2 \times T_{e2}$) in converting this operating point to a new one with velocity ω_2 and electromagnetic torque T_{e2}. Thus, the working condition change is to change the power supplied to the motor from the inverter.

Changing the rotor speed cannot be instantaneous but takes a short time with a specific route. During this process, the inverter's power can change with the principle that if the power increases, the speed will increase, and vice versa.

When the rotor rotates once, the permanent magnet's magnetic field will sweep Pp times the number of coils on it. Thus, the BEMF generated when the permanent magnet's magnetic field turns with the speed ω_m induced on the stator coil is determined by Faraday's induction law (12).

$$E = Pp \times \omega_m \times \lambda_{pm} \tag{12}$$

With the synchronous motor in the stationary state, the magnetic field speed equals the rotor speed, $\omega_e = \omega_m \times Pp$. The Equation (12) is rewritten according to the stator magnetic field rate, as shown in (8).

$$E = \omega_e \times \lambda_{pm} \tag{13}$$

When two alternating current sources have the same rotating speed of the magnetic field, based on recommendations in [33], Figure 3 represented the equivalent circuit of these two voltage sources.

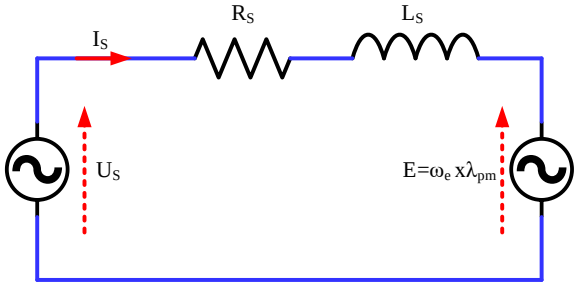

Figure 3. Equivalent circuit of PMSM in steady-state [33].

According to Figure 1, the transparent power transmitted to the BEMF terminal is determined according to (14) with the current determined according to (15):

$$S = 3 \times E \times I_S \tag{14}$$

$$I_S = \frac{|U_S|\angle\delta - |E|\angle 0^0}{|Z_S|\angle\beta} \tag{15}$$

From Equations (14) and (15), we get

$$S = 3\frac{|U_S| \times |E|}{|Z_S|}\angle(\beta - \delta) - 3\frac{|E|^2}{|Z_S|}\angle\beta \tag{16}$$

The active and reactive power is derived from (16) and determined according to (17) and (18) respectively.

$$P = 3\frac{|U_S| \times |E|}{|Z_S|}\cos(\beta - \delta) - 3\frac{|E|^2}{|Z_S|}\cos\beta \tag{17}$$

$$Q = 3\frac{|U_S| \times |E|}{|Z_S|}\sin(\beta - \delta) - 3\frac{|E|^2}{|Z_S|}\sin\beta \tag{18}$$

If resistance is neglected, then $Zs = X_L$ and $\beta = 90^\circ$. At this time, Equations (17) and (18) are rewritten as (19) and (20), respectively, as follows.

$$P = 3\frac{|U_S| \times |E|}{X_L}\sin\delta \tag{19}$$

$$Q = 3\frac{|E|}{X_L}(|U_S|\cos\delta - |E|) \tag{20}$$

The active power P transmitted between the two voltage sources is determined by the Equation (21) where δ is an angular deviation between the phase of inverters voltage vector and phase of back electromotive force vector in the stator winding, as shown in Figure 4. In order to stabilize PMSM operations under electric motor drive mode, δ is kept within $(0; \pi/2)$.

$$P = 3\frac{|U_S| \times |E| \times \sin\delta}{X_L} \tag{21}$$

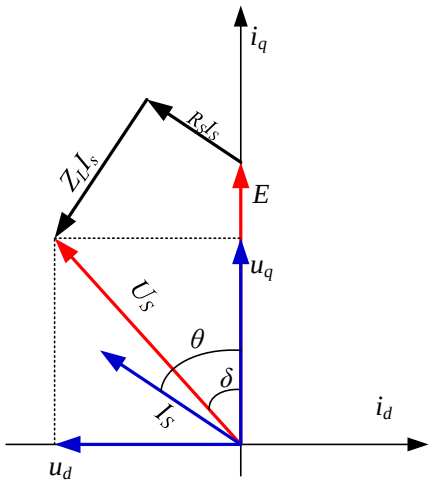

Figure 4. Vector diagram of the voltages on the stator winding in the current plane in the dq axis.

The two voltage sources' impedance value is kept constant in the stationary state, with a constant rotor velocity according to (23), with a new inductance determined according to (10). The amplitude of BEMF is determined based on (13).

$$L = L_d = L_q \tag{22}$$

$$(X_L = \omega_e \times L) \tag{23}$$

Combined with (13) and (23), the power applied to the motor from the inverter is determined according to (24).

$$P = 3\frac{|U_S| \times \lambda_{pm} \times \sin\delta}{L} \tag{24}$$

During operation, L and λ_{pm} have slight changes due to magnetic saturation and magnet temperature. However, in comparison with U_S and δ, this change is not significant and can be ignored. Therefore, we can consider that L and λ_{pm} are constants in the control process. We can calculate transmitted power based on (25) where constant $k = 3 \times \lambda_{pm}/L$.

$$P = k \times |U_S| \times \sin\delta \tag{25}$$

During operation, the inverter provides active power P to the motor. Reactive power Q does not participate in the transfer of energy from the stator to the rotor, but only serves as the power supply for the magnetization of the magnetic circuits. The reactive power Q only plays a specific role in the switching support, so the goal is to minimize the reactive power Q supplied to the BEMF source.

The goal in motor control is zero reactive power QR at the BEMF end. Thus, the reactive power Q at the stator head only compensates for the magnetic circuit's loss. The reactive power Q obtained at the BEMF input is determined according to (20).

For Q = 0, then U_S must satisfy (26).

$$U_S = \frac{E}{\cos\delta} \tag{26}$$

When considering the internal resistance of the stator winding, the voltage drop across the winding is determined as follows:

$$\Delta U = I_s Z = \left(I_d + jI_q\right)\left(R_S + jX_L\right) = \left(I_d R_S - I_q X_L\right) + j\left(I_q R_S + I_d X_L\right) \tag{27}$$

Due to $\left(I_q R_S + I_d X_L\right) \gg \left(I_d R_S - I_q X_L\right)$, it leads to the voltage drop magnitude which is calculated by (28).

$$|\Delta U| \simeq \left(I_q R_S + I_d X_L\right) \tag{28}$$

Combined (26) and (28), the inverter voltage amplitude is calculated according to (29).

$$|U_S| = \left|\frac{E}{\cos\delta}\right| + \left|\left(I_q R_S + I_d \omega_e L\right)\right| \tag{29}$$

Thus, the active power P to change the working point from the point with power P_1 to the operation point with power P_2 is determined by adjusting the inverter voltage range. The angle δ is calibrated to the new working point, so that the reactive power supplied to the BEMF is zero.

3. The Principle of Controlling the Speed of a PMSM Motor Is Based on the Power Control PQ

The control diagram of the PMSM motor is shown in Figure 5 below, based on the control principle analyzed above.

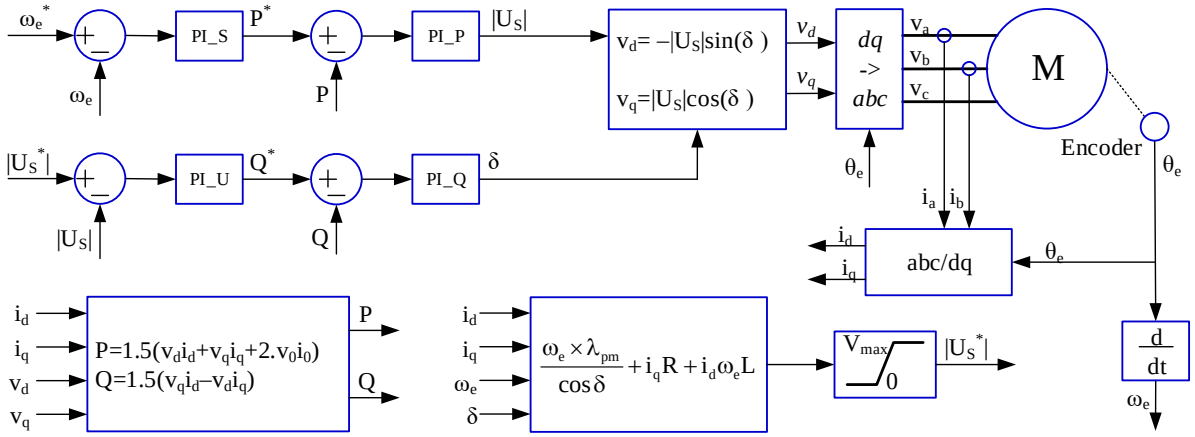

Figure 5. The PMSM speed control principle is based on the active and reactive power control of the inverters.

- The active power is adjusted through the speed PI controller (PI_S) from the actual speed difference compared to the reference speed.
- The power PI controller is used to change the inverter voltage amplitude, to change the power supplied to the inverter according to the reference power,
- To ensure that reactive power Q is not fed to the BEMF source, the inverter voltage must be kept at a value according to (18) and must not exceed the inverter limit value to optimize motor operation. Inverter voltage must be kept at a determined value; some reactive power must be added (or drawn) from the inverters. The determination of reactive power Q is done via a voltage controller with the input of the error between the reference voltage and the actual voltage at the inverter output.
- The reactive power PI controller corrects the voltage angle δ between U and E, respectively, to change the reactive power to the reference value. The BEMF vector angle is always perpendicular to the direction of the d-axis current component, as shown in Figure 4; the voltage across the inverters' coordinate system dq is determined according to (19) and (20).

$$v_d = -|U_S| \sin(\delta) \quad (30)$$

$$v_q = |U_S| \cos(\delta) \quad (31)$$

4. Simulation Validation

4.1. Simulation IPMSM Speed Control Model

The PMSM motor speed control model is built on the simulation software Matlab/Simulink used to evaluate the proposed control efficiency. Table 1 shows the PMSM motors' parameters used in the simulation; these parameters belong to the EMJ-04APB22 motor, which Wang et al. used in their study [34]. The Texas Instruments Company recommends the use of the EMJ-04APB22 motor in the quality assessment of controllers. The model is built with three main blocks, the PMSM motor block, the control unit, and the inverter block Figure 6 shows the simulation PMSM model. The Vector Current Control (VCC) method [35] and the Direct Current Calculation (DCC) method [36] were used to evaluate the proposed control method's effectiveness. The simulation results under different operating conditions are satisfactorily introduced in detail in the following sections.

Table 1. PMSM parameters.

Parameter	Symbol	Value	Unit
Rated power		400	W
Rated phase current	I_{max}	2.7	A_{rms}
Rated speed	ω_{rate}	3000	RPM
Rated torque	T_{rate}	1.27	N.m
Number of poles pairs	P	4	
Stator resistance	R	2.35	Ω
Stator inductance	$L = L_d = L_q$	8.5	mH
Flux linkage	λ_{pm}	0.0615	Wb
Inertia	J	167×10^{-6}	$Kg.m^2$
Viscous friction	F	106.9×10^{-6}	N.m.s/rad
DC Bus Voltage	V_{dc}	200	V

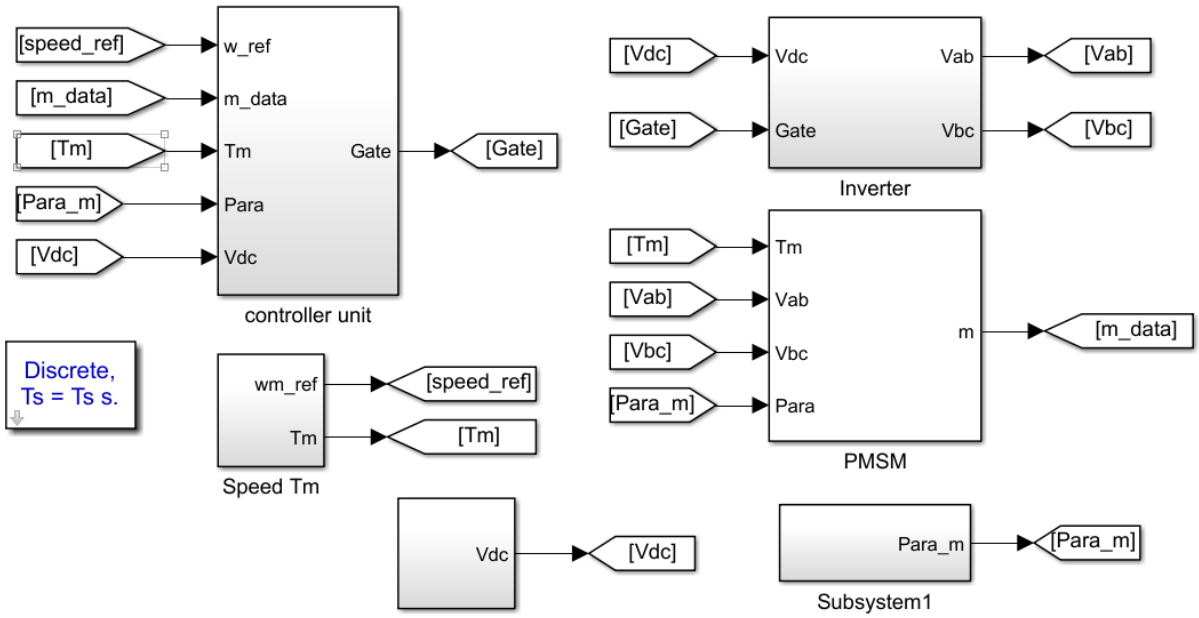

Figure 6. IPMSM control simulation model.

4.2. Simulation Results

The PMSM motor is used to test the proposed method's control quality in constant torque and constant power zones at various speeds. The speed variation between two operating zones, as well as within the same operating region of PMSM, is used to evaluate the effect of extending the operating speed range and minimizing the fluctuations in electric torque, current, and associated flux of PMSM in the FW region of the proposed method. Figure 7 shows the speed control results. The obtained results show that the control methods can adhere well to the reference speed.

The under-rated speed enlargement results show that DCC and VCC control methods got lower overshoot than the proposed method. The reason for this is that when controlling the constant torque region, it is much more efficient to change the speed by changing the current when having to indirectly control the speed by holding power inject to the motor. Although the response is slower, the proposed method is more stable, with the speed's ripple less than the other DCC and VCC ways.

The speed enlargement results in the FW region show that the two DCC and VCC methods also have a lower overshoot than the proposed method. However, these two methods' speed ripple is much higher, and thus the quality of speed control is also significantly reduced. The reason is that when entering the voltage limit area, the method of current management and voltage correction through the current controller will no longer

be as effective as in the constant torque region. Then, the proposed method shows the advantages when the two control zones' speed control quality is the same and stable.

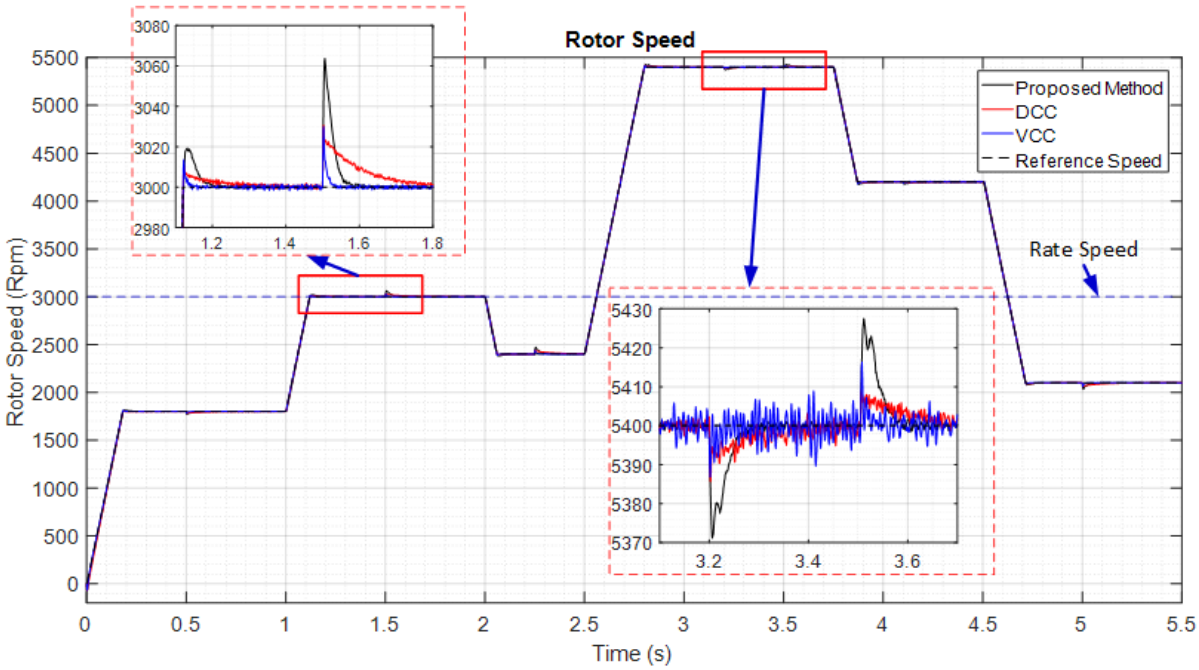

Figure 7. Comparative speed control results of PMSM.

Figure 8a shows the results of the electromagnetic moment of comparative control methods. The simulation results show that all three approaches give a small ripple in the constant moment region. Electromagnetic torque responds to changes in the load torque and the need for the engine's acceleration or deceleration speed. Figure 8b shows electromagnetic moment results at a constant power range. The electromagnetic moment oscillation of VCC, DCC and the proposed approach is (0.35–0.6) N.m, (0.38–0.5) N.m, (0.42–0.48) N.m, respectively. The result of the flux linkage ripple percent is 26.3%, 13.64%, and 6.67%, respectively. This means that the VCC and DCC methods' electromagnetic torque has a more significant ripple than the proposed method while entering the FW region. The results demonstrate the proposed method's ability to minimize the electromagnetic torque ripple. The task of reducing electromagnetic surges plays a crucial role in improving not only the control quality but also the electric drive system's stability.

The stator winding power loss is determined based on the stator current and stator resistance, as shown in (21). Figure 9 shows the power loss simulation results. The results show that the proposed control method has the same effect of minimizing losses as the other comparative methods. These results show that the proposed control method effectively reduces power loss as the current-based control method, similar to the FOC control method.

$$P_{loss} = I_s^2.R_s \quad (32)$$

Figure 10a shows the flux linkage results. The flux linkage in the control method is greater than that of the flux linkage of the permanent magnet when operating in the constant torque region. The flux linkage decreases when entering the constant power region. Figure 10b shows the flux linkage results at a constant power range. It is important to note that flux linkage oscillation of VCC, DCC and the proposed approach is (0.038–0.045) Wb, (0.04–0.043) Wb, (0.04–0.041) Wb, respectively. This leads to the flux linkage ripple percentage, at 18%, 7.5%, and 2.5%, respectively. Hence, the VCC and DCC methods' flux linkage value has a more significant ripple than the proposed method.

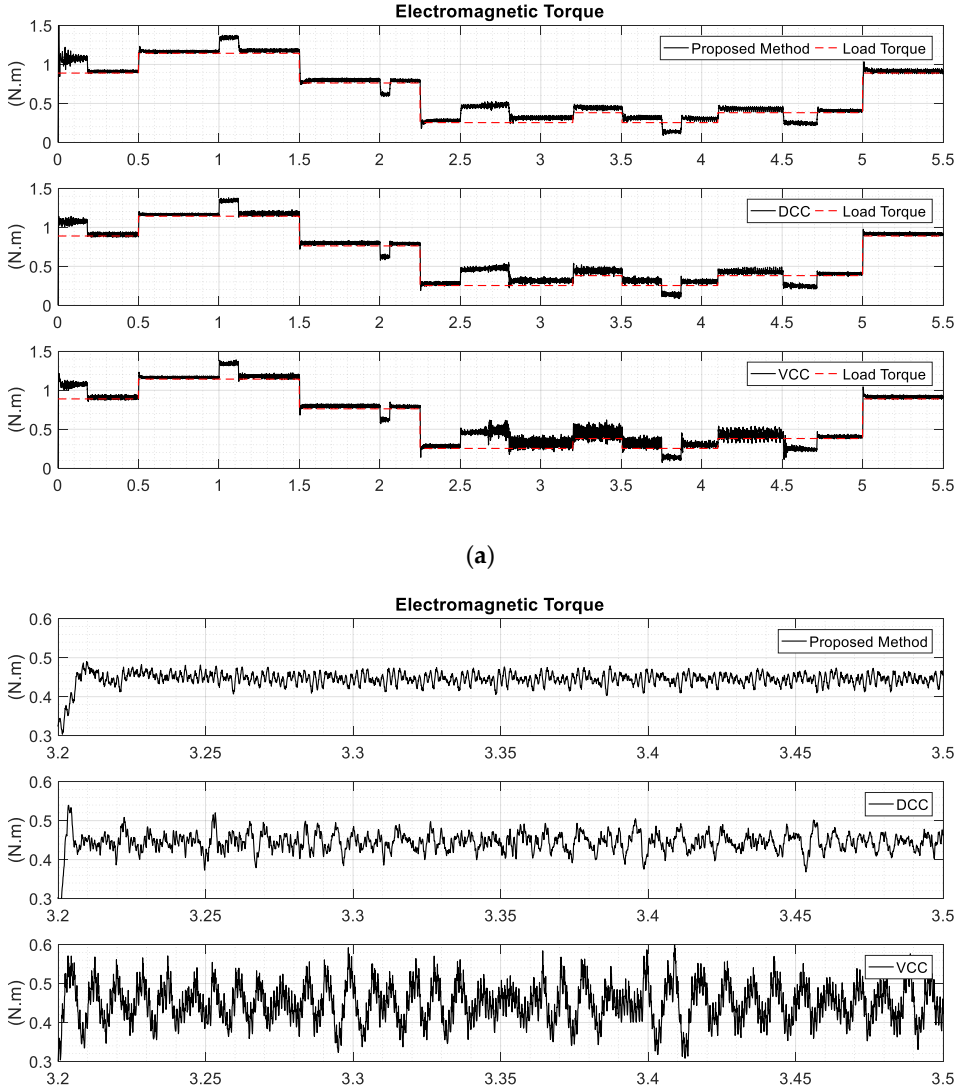

Figure 8. Comparative Electromagnetic Torque results of PMSM in (**a**) full simulation time range and (**b**) interval time of (3.2–3.5 s).

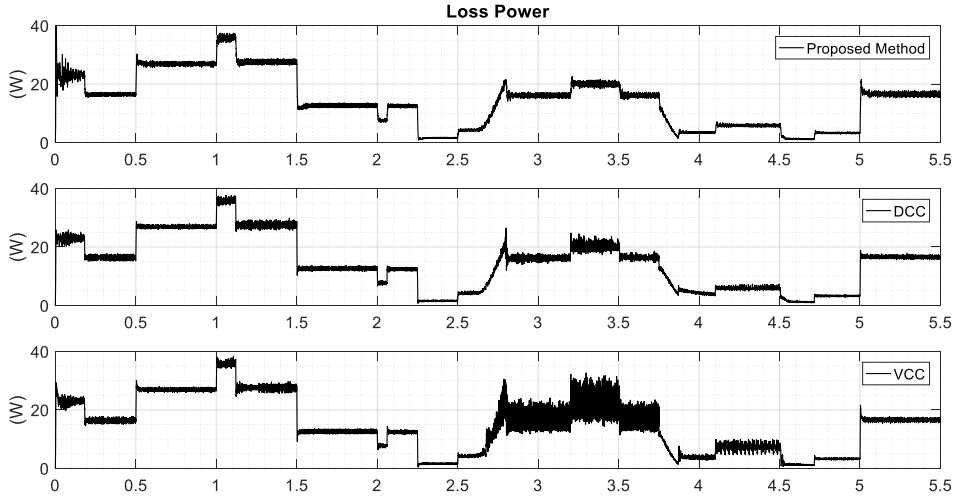

Figure 9. Comparative power loss results of PMSM.

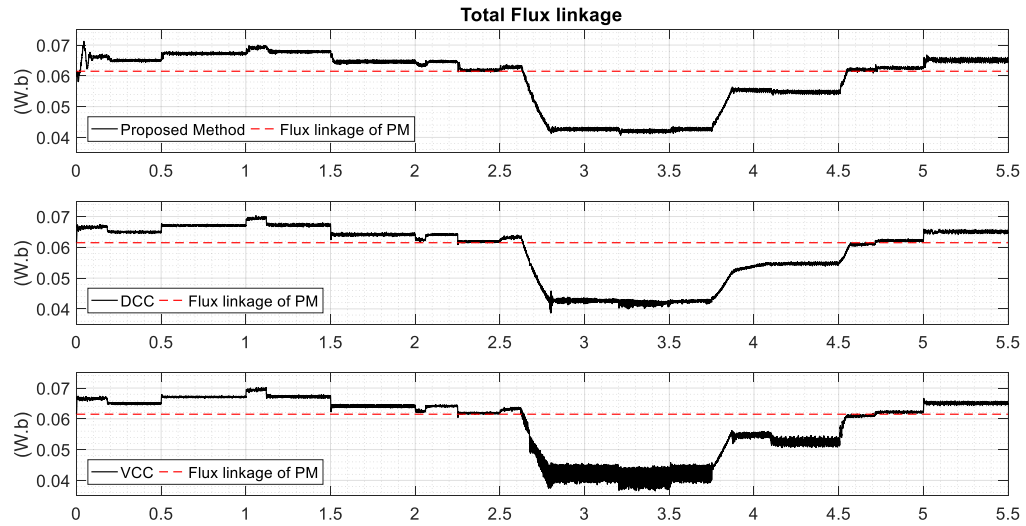

(**a**)

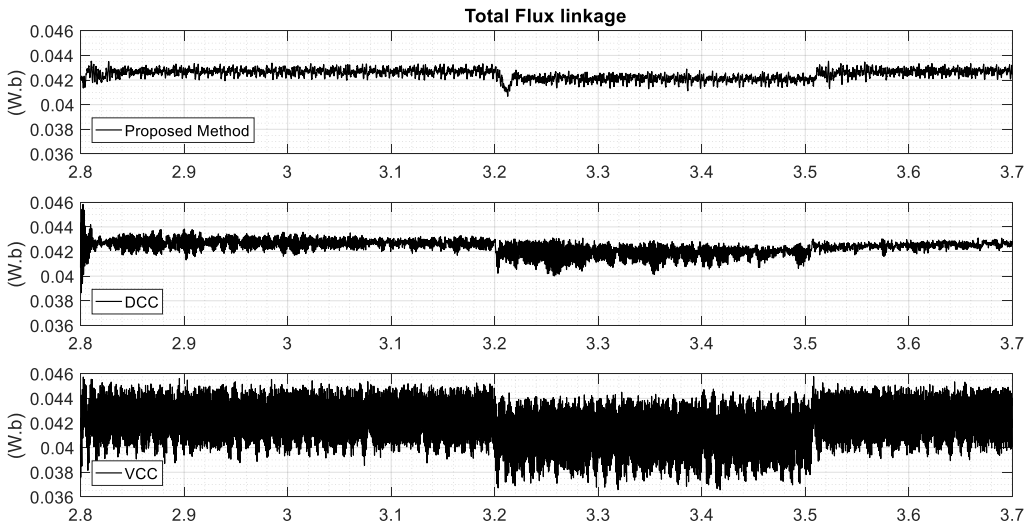

(**b**)

Figure 10. Comparative Total Flux linkage results of PMSM in (**a**) full simulation time range and (**b**) interval time of (2.8–3.7 s).

Figure 11a shows the resulting stator currents controlled by different methods. The similarity of the currents within the constant moment range can be seen immediately. However, when entering the FW region, the quality of the stator current has a big difference. Zooming in on these results in Figure 11b from 3.2 s to 3.5 s shows the difference between the comparative methods. The current fluctuation of the VCC method is the most significant (2.4–3.3) A, with a fluctuation rate of 15.8%. On the contrary the current instability of the proposed method is the smallest (2.6–2.8) A, with a fluctuation rate of 3.7%. Hence, a current ripple of the proposed method is significantly smaller than two other comparative approaches in the FW mode.

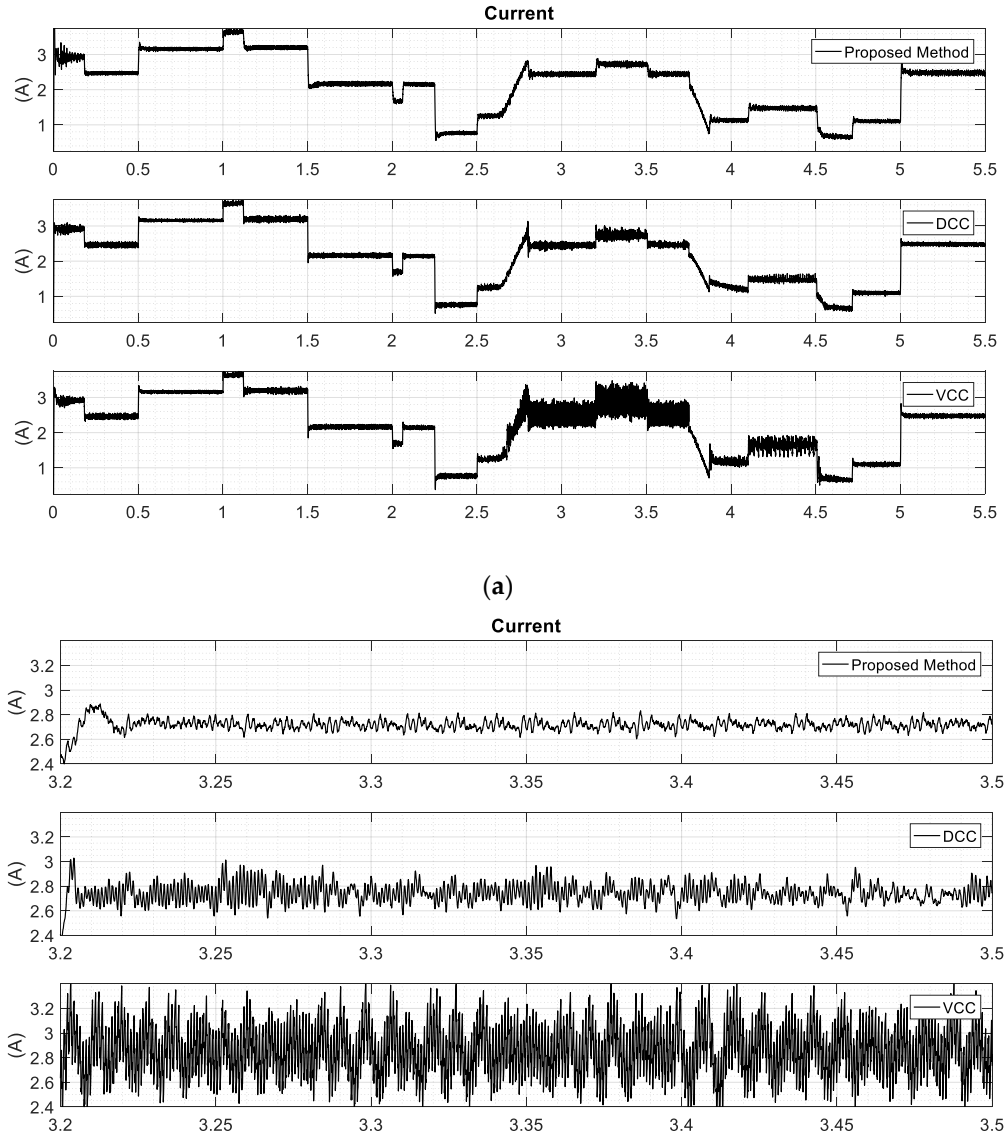

Figure 11. Comparative current results of PMSM in (**a**) full simulation time range and (**b**) interval time of (3.2–3.5 s).

Figure 12 shows the voltage simulation results on the stator winding. The recorded results show that the proposed method's voltage is more stable than the DCC and VCC methods when operating in the FW region. In the area of the constant moment, the ripple of the current and voltage amplitude is equivalent. Moreover, it also shows the superiority of the proposed method in expanding the range of PMSM operating speeds in comparison with the DCC and VCC control methods.

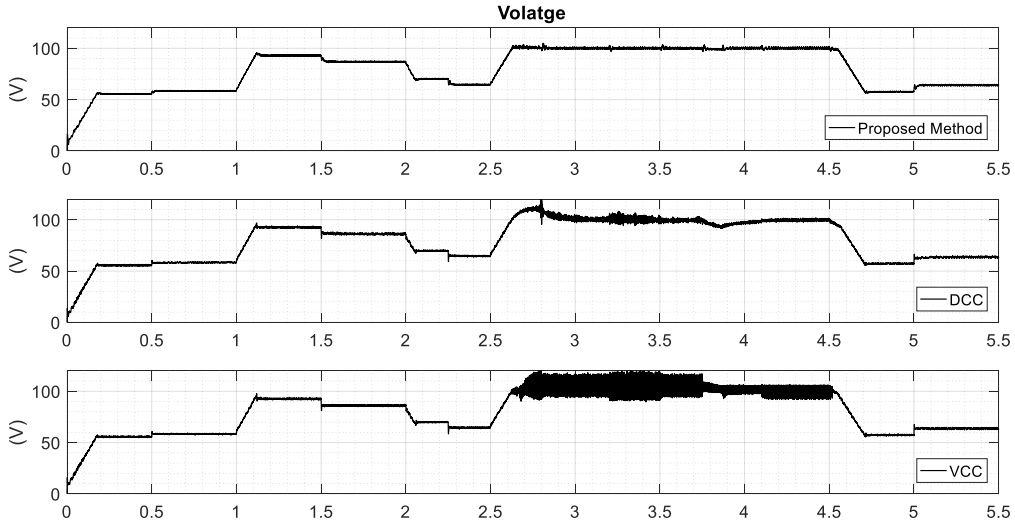

Figure 12. Comparative Voltage results of PMSM.

5. Conclusions

The paper proposes an advanced method to expand the PMSM speed range by controlling the inverter power instead of the conventional current control approach. Speed control based on power balance allows flexible control, no longer considering higher or lower rotor speed conditions along with switch control strategies. After comprehensive simulations, it is possible to state that the proposed control method is capable of stable operation from 300 to 5500 rpm, regardless of changing the PMSM speed control method between two separate working stages: the constant power region and constant torque region. By controlling the power injected into the PMSM, the proposed control method allows for reasonable control of the storage systems' discharge power, necessary in mobile drive applications. The proposed control method contains the same number of control loops, and does not need to provide any additional data compared to the two comparative control methods. In comparing simulation results with the two traditional DCC and VCC control methods, the proposed control method has proven to improve not only control quality and stability, but also to minimize electromagnetic torque and current ripples. The fact is that, during PMSM operation, the algorithm uses PMSM parameters to calculate the voltage to be supplied by the inverter, which leads to the requirement of accurately determining PMSM parameters. These limitations lead to the subsequent development direction of the research, to further improve the control efficiency of the proposed PMSM speed control algorithm.

Author Contributions: Conceptualization, P.Q.K. and V.-A.T.; methodology, P.Q.K.; software, P.Q.K.; validation, H.P.H.A.; formal analysis, P.Q.K. and V.-A.T.; investigation, H.P.H.A.; resources, P.Q.K.; data curation, P.Q.K.; writing—original draft preparation, P.Q.K.; writing—review and editing, H.P.H.A.; visualization, P.Q.K.; supervision, H.P.H.A.; project administration, H.P.H.A.; funding acquisition, H.P.H.A. This paper was a collaborative effort among all authors. All authors conceived the methodology, conducted the performance tests, and wrote the article. All authors have read and agreed to the published version of the manuscript.

Funding: This research received no external funding.

Institutional Review Board Statement: Not applicable.

Informed Consent Statement: Not applicable.

Data Availability Statement: Not applicable.

Acknowledgments: We acknowledge the support of the time and facilities of the Ho Chi Minh City University of Technology (HCMUT), VNU-HCM, for this study.

Conflicts of Interest: The authors declare no conflict of interest.

Nomenclature

v_d (v_q)	Stator voltage in d–q coordinate system
i_d (i_q)	Stator current in d–q coordinate system
L_d (L_q)	stator inductance in dq coordinate system
λ_{pm}	Magnet flux linkage
R_S	Stator resistance
Ω	rotor speed
ω_e	magnetic field speed
P_p	number of pole pairs
T_e	Electromagnetic torque
J	The inertia of motor and load combined reduced to the motor shaft.
F	The combined viscous friction coefficient of rotor and load.
θ	Rotor angular position
T_L	Shaft load torque
θ_m	Angular velocity of the rotor (mechanical speed)
P_1, P_2	Power at the inverter output
E	back electromotive force in the stator winding
S	transparent power transmitted to the back electromotive force terminal
P	Active power transmitted to the back electromotive force terminal
Q	Reactive power transmitted to the back electromotive force terminal
$\|Us\|$	Voltage amplitude at the inverter output
φ_{us}	the phase of inverters voltage vector
φ_E	the phase of back electromotive force in the stator winding
δ	angular deviation between φus and φE
β	Phase of winding impedance
X_L	Winding impedance
L	winding inductance
ΔU	voltage drop across the winding

References

1. Tang, Z.; Akin, B. A New LMS Algorithm Based Deadtime Compensation Method for PMSM FOC Drives. *IEEE Trans. Ind. Appl.* **2018**, *54*, 6472–6484. [CrossRef]
2. Cash, S.; Olatunbosun, O. Fuzzy logic field-oriented control of an induction motor and a permanent magnet synchronous motor for hybrid/electric vehicle traction applications. *Int. J. Electr. Hybrid Veh.* **2017**, *9*, 269–284. [CrossRef]
3. Lara, J.; Chandra, A. Performance investigation of two novel HSFSI demodulation algorithms for encoderless FOC of PMSMs intended for EV propulsion. *IEEE Trans. Ind. Electron.* **2017**, *65*, 1074–1083. [CrossRef]
4. Lu, D.; Ouyang, M.; Gu, J.; Li, J. Optimal Velocity Control for a Battery Electric Vehicle Driven by Permanent Magnet Synchronous Motors. *Math. Probl. Eng.* **2014**, *2014*, 1–14. [CrossRef]
5. Samat, A.A.A.; Zainal, M.; Ismail, L.; Saidon, W.S.; Tajudin, A.I. Current PI-Gain Determination for Permanent Magnet Synchronous Motor by using Particle Swarm Optimization. Indones. *J. Electr. Eng. Comput. Sci.* **2017**, *6*, 412. [CrossRef]
6. Amin, F.; Sulaiman, E.B.; Utomo, W.M.; Soomro, H.A.; Jenal, M.; Kumar, R. Modelling and Simulation of Field Oriented Control based Permanent Magnet Synchronous Motor Drive System. Indones. *J. Electr. Eng. Comput. Sci.* **2017**, *6*, 387. [CrossRef]
7. Mesloub, H.; Benchouia, M.T.; Goléa, A.; Goléa, N.; Benbouzid, M.E.H. Predictive DTC schemes with PI regulator and particle swarm optimization for PMSM drive: Comparative simulation and experimental study. *Int. J. Adv. Manuf. Technol.* **2016**, *86*, 3123–3134. [CrossRef]
8. Ghamri, A.; Boumaaraf, R.; Benchouia, M.T.; Mesloub, H.; Goléa, A.; Goléa, N. Comparative study of ANN DTC and conventional DTC controlled PMSM motor. *Math. Comput. Simul.* **2020**, *167*, 219–230. [CrossRef]
9. Guven, S.; Usta, M.A.; Okumus, H.I. An improved sensorless DTC-SVM for three-level inverter-fed permanent magnet synchronous motor drive. *Electr. Eng.* **2018**, *100*, 2553–2567. [CrossRef]
10. Ouledali, O.; Meroufel, A.; Wira, P.; Bentouba, S. Direct Torque Fuzzy Control of PMSM based on SVM. *Energy Procedia* **2015**, *74*, 1314–1322. [CrossRef]
11. Mendoza-Mondragõn, F.; Hernández-Guzmán, V.M.; Carrillo-Serrano, R.V. Velocity regulation in pmsms using standard field oriented control plus adaptation. *Asian J. Control* **2015**, *17*, 2382–2388. [CrossRef]
12. Shihua, L.; Zhigang, L. Adaptive Speed Control for Permanent-Magnet Synchronous Motor System with Variations of Load Inertia. *IEEE Trans. Ind. Electron.* **2009**, *56*, 3050–3059. [CrossRef]

13. Guan, Y.; Zhu, Z.; Afinowi, I.; Mipo, J. Influence of machine design parameters on flux-weakening performance of induction machine for electrical vehicle application. *IET Electr. Syst. Transp.* **2015**, *5*, 43–52. [CrossRef]
14. Dong, Z.; Yu, Y.; Li, W.; Wang, B.; Xu, D. Flux-Weakening Control for Induction Motor in Voltage Extension Region: Torque Analysis and Dynamic Performance Improvement. *IEEE Trans. Ind. Electron.* **2018**, *65*, 3740–3751. [CrossRef]
15. Xu, Y.; Morito, C.; Lorenz, R.D. Extending High-Speed Operating Range of Induction Machine Drives Using Deadbeat-Direct Torque and Flux Control With Precise Flux Weakening. *IEEE Trans. Ind. Appl.* **2019**, *55*, 3770–3780. [CrossRef]
16. Aghdam, M.G.H. Z-Source Inverter with SiC Power Semiconductor Devices for Fuel Cell Vehicle Applications. *J. Power Electron.* **2011**, *11*, 606–611. [CrossRef]
17. Rahmani, F.; Quispe, D.; Agarwal, T.; Barzegaran, M. Speed Control of Brushless DC Motor by DC-DC Boost and Buck Converters Using GaN and SiC Transistors for Implementing the Electric Vehicles. *MPRA* **2020**, *6*, 70–75.
18. Liu, T.-H.; Tseng, S.-K.; Lu, M.-B. Auto-tuning flux-weakening control for an IPMSM drive system using a predictive controller. In Proceedings of the 2017 IEEE 26th International Symposium on Industrial Electronics (ISIE), Edinburgh, UK, 19–21 June 2017; Volume 2, pp. 238–243. [CrossRef]
19. Bedetti, N.; Calligaro, S.; Petrella, R. Analytical design and auto-tuning of adaptive flux-weakening voltage regulation loop in IPMSM drives with accurate torque regulation. *IEEE Trans. Ind. Appl.* **2019**. [CrossRef]
20. Agarwal, T.; Rahmani, F.; Zaman, I.; Gasbarri, F.; Davami, K.; Barzegaran, M. Comprehensive design analysis of a 3D printed sensor for readiness assessment applications. *COMPEL-Int. J. Comput. Math. Electr. Electron. Eng.* **2021**. [CrossRef]
21. Wang, C.; Zhu, Z.Q. Fuzzy Logic Speed Control of Permanent Magnet Synchronous Machine and Feedback Voltage Ripple Reduction in Flux-Weakening Operation Region. *IEEE Trans. Ind. Appl.* **2020**, *56*, 1505–1517. [CrossRef]
22. Wang, M.-S.; Hsieh, M.-F.; Lin, H.-Y. Operational Improvement of Interior Permanent Magnet Synchronous Motor Using Fuzzy Field-Weakening Control. *Electronics* **2018**, *7*, 452. [CrossRef]
23. Cao, X.; Fan, L. Flux-Weakening Control Scheme Based on the Fuzzy Logic of PMSM Drive for Hybrid Electric Vehicle. In Proceedings of the 2009 IITA International Conference on Control, Automation and Systems Engineering (Case 2009), Zhangjiajie, China, 11–12 July 2009; pp. 287–290. [CrossRef]
24. Uddin, M.N.; Rahman, M.A. High-Speed Control of IPMSM Drives Using Improved Fuzzy Logic Algorithms. *IEEE Trans. Ind. Electron.* **2007**, *54*, 190–199. [CrossRef]
25. Wang, H.; Wang, T.; Zhang, X.; Guo, L. Voltage feedback based flux-weakening control of IPMSMs with fuzzy-PI controller. *Int. J. Appl. Electromagn. Mech.* **2020**, *62*, 31–43. [CrossRef]
26. Gu, X.; Li, T.; Li, X.; Zhang, G.; Wang, Z. An Improved UDE-Based Flux-Weakening Control Strategy for IPMSM. *Energies* **2019**, *12*, 4077. [CrossRef]
27. Stojan, D.; Drevensek, D.; Plantic, Ž.; Grcar, B.; Stumberger, G. Novel Field-Weakening Control Scheme for Permanent-Magnet Synchronous Machines Based on Voltage Angle Control. *IEEE Trans. Ind. Appl.* **2012**, *48*, 2390–2401. [CrossRef]
28. Xiaochun, F.; Fei, L.; Zhongping, Y. A modified flux-weakening control method of PMSM based on the d-q current cross-coupling effect. In Proceedings of the 2014 IEEE Conference and Expo Transportation Electrification Asia-Pacific (ITEC Asia-Pacific), Beijing, China, 31 August–3 September 2014; pp. 1–6. [CrossRef]
29. Zhang, Z.; Wang, C.; Zhou, M.; You, X. Flux-Weakening in PMSM Drives: Analysis of Voltage Angle Control and the Single Current Controller Design. *IEEE J. Emerg. Sel. Top. Power Electron.* **2019**, *7*, 437–445. [CrossRef]
30. Li, X.; Liu, C.; Wu, S.; Chi, S.; Loh, P.C. Sliding-Mode Flux-Weakening Control With Only Single Current Regulator for Permanent Magnet Synchronous Motor. *IEEE Access* **2019**, *7*, 131616–131626. [CrossRef]
31. Lei, Z.; Xuhui, W.; Feng, Z.; Liang, K.; Baocang, Z. Deep field-weakening control of PMSMs for both motion and generation operation. In Proceedings of the 2011 International Conference on Electrical Machines and Systems, Beijing, China, 20–23 August 2011; Volume 4, pp. 1–5. [CrossRef]
32. Xu, W.; Ismail, M.M.; Liu, Y.; Islam, M.R. Parameter Optimization of Adaptive Flux-Weakening Strategy for Permanent-Magnet Synchronous Motor Drives Based on Particle Swarm Algorithm. *IEEE Trans. Power Electron.* **2019**, *34*, 12128–12140. [CrossRef]
33. Dambrauskas, K.; Vanagas, J.; Zimnickas, T.; Kalvaitis, A.; Ažubalis, M. Method for Efficiency Determination of Permanent Magnet Synchronous Motor. *Energies* **2020**, *13*, 1004. [CrossRef]
34. Wang, S.; Kang, J.; Degano, M.; Galassini, A.; Gerada, C. An Accurate Wide-Speed Range Control Method of IPMSM Considering Resistive Voltage Drop and Magnetic Saturation. *IEEE Trans. Ind. Electron.* **2020**, *67*, 2630–2641. [CrossRef]
35. Bolognani, S.; Calligaro, S.; Petrella, R. Adaptive Flux-Weakening Controller for Interior Permanent Magnet Synchronous Motor Drives. *IEEE J. Emerg. Sel. Top. Power Electron.* **2014**, *2*, 236–248. [CrossRef]
36. Fornari, R.; Franceschini, G.; David, D.; Torreggiani, A.; Bianchini, C.; Frigieri, M. Enhanced Internal Permanent-Magnet Machines Flux Weakening Control Strategies for Traction Applications. In Proceedings of the IECON 2019-45th Annual Conference of the IEEE Industrial Electronics Society, Lisbon, Portugal, 14–17 October 2019; Volume 1, pp. 2682–2687. [CrossRef]